Langmuir
Article
pubs.acs.org/Langmuir

Self-Assembled Template-Directed Synthesis of One-Dimensional Silica and Titania Nanostructures

Handan Acar, Ruslan Garifullin, and Mustafa O. Guler*

UNAM-Institute of Materials Science and Nanotechnology, Bilkent University, Ankara, Turkey 06800

Received July 30, 2010

Mineralized biological materials such as shells, skeleton, and teeth experience biomineralization. Biomimetic materials exploit the biomineralization process to form functional organic−inorganic hybrid nanostructures. In this work, we mimicked the biomineralization process by the de novo design of an amyloid-like peptide that self-assembles into nanofibers. Chemically active groups enhancing the affinity for metal ions were used to accumulate silicon and titanium precursors on the organic template. The self-assembly process and template effect were characterized by CD, FT-IR, UV−vis, fluorescence, rheology, TGA, SEM, and TEM. The self-assembled organic nanostructures were exploited as a template to form high-aspect-ratio 1-D silica and titania nanostructures by the addition of appropriate precursors. Herein, a new bottom-up approach was demonstrated to form silica and titania nanostructures that can yield wide opportunities to produce high-aspect-ratio inorganic nanostructures with high surface areas. The materials developed in this work have vast potential in the fields of catalysis and electronic materials.

Introduction

Self-assembled amyloid-like peptides[1] have emerged as a unique class of materials with potential applications as templates for nanotube[2] and nanowire[3,4] growth, 1-D nanostructure organization,[5] micromechanical system components,[6] and interconnects for nanoelectronics.[7] Amyloid-like peptides provide suitable conditions for the template-directed mineralization process with their inherent ability to self-assemble into fibrillar nanostructures.[8,9] These organic−inorganic hybrid materials are important in the bottom-up synthesis of 1-D inorganic nanostructures.

Organic materials and polymers are strongly integrated into modern technology; nevertheless, inorganic materials preserve their status as basic elements in engineering. However, there is increasing awareness that the conventional methods of "heat and beat" have several limitations in fulfilling the requirements of future advanced materials, in particular, the construction of complex architectures from the nanoscale to the macroscale; this knowledge creates a vital need for novel synthesis methods. There is no doubt that new approaches using conceptually new solutions, such as biomimetic design and self-assembly, should be developed and used to expand the frontiers of possibility in this field. The ability of biomimetic materials to organize inorganic "bricks" into nanoscale, microscale, and macroscale materials has great potential in electronics,[10,11] catalysis,[12,13] sensors,[14] molecular recognition,[15] magnetism,[16−18] optics,[19] photonics,[20] and biomedical applications.[21]

In this work, we designed and synthesized an amyloid-like peptide (ALP) and studied the mineralization of preformed nanofibers composed of ALP molecules for the fabrication of 1-D silica (SiO_2) and titania (TiO_2) nanostructures. The self-assembly of peptides was achieved by a specially designed short peptide sequence, Ac-KFFAAK-Am (Figure 1), that forms sheetlike hydrogen-bonded structures. Functional groups on side chains of lysine residues served as nucleation centers for the successive deposition of inorganic precursor materials. The transformation of deposited material to target inorganic material and the removal of organic templates were achieved by a calcination process at an appropriate temperature. The simple preparation process of targeted inorganic materials makes the ALP-templated process very lucrative not only for laboratory-scale preparation but also for industrial large-scale applications.

Experimental Section

Peptide Synthesis. Fmoc- and Boc-protected amino acids, MBHA rink amide resin, and HBTU were purchased from NovaBiochem and ABCR. The other chemicals were purchased from Fisher, Merck, Alfa Aesar, and Aldrich and were used as

*Corresponding author. E-mail: moguler@unam.bilkent.edu.tr. Tel: +90 (312) 290 3552. Fax: +90 (312) 266 4365.

(1) MacPhee, C. E.; Woolfson, D. N. *Curr. Opin. Solid State Mater.* **2004**, *8*, 141–149.
(2) Carny, O.; Shalev, D. E.; Gazit, E. *Nano Lett.* **2006**, *6*, 1594–1597.
(3) Reches, M.; Gazit, E. *Science* **2003**, *300*, 625–627.
(4) Scheibel, T.; Parthasarathy, R.; Sawicki, G.; Lin, X.-M.; Jaeger, H.; Lindquist, S. L. *Proc. Natl. Acad. Sci. U.S.A.* **2003**, *100*, 4527–4532.
(5) Zhao, Y. S.; Fu, H.; Peng, A.; Ma, Y.; Xiao, D.; Yao, J. *Adv. Mater.* **2008**, *20*, 2859–2876.
(6) Banerjee, P.; Perez, I.; Henn-Lecordier, L.; Lee, S. B.; Rubloff, G. W. *Nat. Nanotechnol.* **2009**, *4*, 292–296.
(7) Wang, C.-J.; Lin, L. *Nanoscale Res. Lett.* **2007**, *2*, 219–229.
(8) Gazit, E. *Prion* **2007**, *1*, 32–35.
(9) Gilead, S.; Gazit, E. *Supramol. Chem.* **2005**, *17*, 87–92.
(10) Matsui, H.; Pan, S.; Gologan, B.; Jonas, S. H. *J. Phys. Chem. B* **2000**, *104*, 9576–9579.
(11) Banerjee, I. A.; Yu, L.; Matsui, H. *Proc. Natl. Acad. Sci. U.S.A.* **2003**, *100*, 14678–14682.
(12) Song, Y. J.; Challa, S. R.; Medforth, C. J.; Qiu, Y.; Watt, R. K.; Pena, D.; Miller, J. E.; van Swol, F.; Shelnutt, J. A. *Chem. Commun.* **2004**, *9*, 1044–1045.
(13) Ji, Q. M.; Shimizu, T. *Chem. Commun.* **2005**, *35*, 4411–4413.
(14) Djalali, R.; Chen, Y.-f.; Matsui, H. *J. Am. Chem. Soc.* **2002**, *124*, 13660–13661.
(15) Zhao, Z.; Banerjee, I. A.; Matsui, H. *J. Am. Chem. Soc.* **2005**, *127*, 8930–8931.
(16) Klem, M. T.; Young, M.; Douglas, T. *Mater. Today* **2005**, *8*, 28–37.
(17) Jung, J. H.; Rim, J. A.; Lee, S. J.; Lee, S. S. *Chem. Commun.* **2005**, *4*, 468–470.
(18) Klem, M. T.; Resnick, D. A.; Gilmore, K.; Young, M.; Idzerda, Y. U.; Douglas, T. *J. Am. Chem. Soc.* **2007**, *129*, 197–201.
(19) Banerjee, I. A.; Yu, L.; Matsui, H. *J. Am. Chem. Soc.* **2005**, *127*, 16002–16003.
(20) Mizeikis, V.; Juodkazis, S.; Marcinkevicius, A.; Matsuo, S.; Misawa, H. *J. Photochem. Photobiol., C* **2001**, *2*, 35–69.
(21) Toprak, M. S.; McKenna, B. J.; Mikhaylova, M.; Waite, J. H.; Stucky, G. D. *Adv. Mater.* **2007**, *19*, 1362–1368.

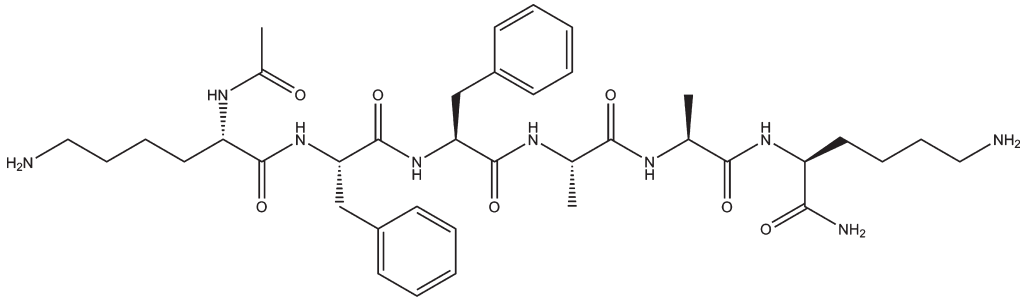

Figure 1. Ac-KFFAAK-Am, an amyloid-like peptide (ALP) sequence.

received without any purification. Peptides were constructed on MBHA rink amide resin. Amino acid coupling reactions were performed with 2 equiv of Fmoc-protected amino acid, 1.95 equiv of HBTU, and 3 equiv of DIEA for 2 h. The Fmoc protecting group removal was performed with a 20% piperidine/DMF solution for 20 min. Cleavage of the peptides from the resin was carried out with 95:2.5:2.5 TFA/TIS/H_2O for 3 h. Excess TFA was removed by rotary evaporation. The remaining peptide was triturated with ice-cold diethyl ether, and the resulting white precipitate was freeze dried. The peptide was characterized by quadruple-time-of-flight mass spectrometry (Q-TOF MS) (Figure S1). The mass spectrum shows the corresponding mass of the peptide; the purity of the peptide was assessed by RP-HPLC and was found to be more than 95% (Figure S2).

Liquid Chromatography−Mass Spectrometry (LC-MS). One milligram of the ALP was added to 1 mL of doubly distilled H_2O and sonicated for 15 min. LC/MS measurements were performed on an Agilent Technologies 1200/6530 Accurate-Mass Q-TOF LC/MS. An Agilent Zorbax Extend-C18 column (rapid resolution HT 2.1 × 50 mm^2, 1.8 μm) was used with gradients of water (0.1% formic acid) and acetonitrile (0.1% formic acid).

UV−Vis and Fluorescence. An ALP solution (3.99×10^{-4} M) was prepared and added to a 1 cm quartz cuvette. UV absorbance measurements were performed on a Varian Cary 100 UV−vis spectrophotometer. Fluorescence measurements were performed on a Varian Cary Eclipse fluorescence spectrophotometer.

FT-IR. Peptide solutions (1.33×10^{-2} M) were prepared in ethanol, methanol, and H_2O at pH 5 and 10. Ethanol and methanol solvents were evaporated in a vacuum oven at 38 °C and 400 mbar for 12 h and then 20 mbar for 12 h. The samples prepared in H_2O were lyophilized for 2 days. One milligram of the remaining powder was mixed with 100 mg of KBr to preparing pellets. A Bruker Tenson 27 FT-IR spectrometer was used for FT-IR analysis in the range of 400−4000 cm^{-1}.

Circular Dichroism (CD). A 3.99×10^{-4} M ALP solution was prepared in different solvents and at different pH values. A Jasco J-815 CD spectrophotometer was used for CD analysis.

Calcination Process. The ALP nanostructures were mineralized by Ti(O-*i*-Pr)$_4$ and TEOS separately. Silica samples were incubated for 1 week at room temperature. Each 100 μL sample was cast on a steel mesh and dried with a critical-point dryer. The titania samples were incubated for 1 h. The mineralized samples were placed in an oven. The oven started to heat up from room temperature to 350 °C at a heating rate of 7 °C/min. The silica samples were incubated at 350 °C for 10 min, and the titania samples were incubated at 450 °C for 10 min.

Scanning Electron Microscopy/Energy-Dispersive X-ray Analysis (SEM/EDX). An FEI Nova 600i Nanolab scanning electron microscope with an EDAX energy-dispersive spectrometer was used. Samples calcined on silicon wafers were used for analysis.

Environmental Scanning Electron Microscopy (E-SEM). E-SEM experiments were performed with an FEI Quanta 200 FEG. Small amounts of samples (ca. 5 μL) were cast on clean silicon wafer. The samples were dried with a critical-point dryer prior to analysis.

Cryo-SEM. An FEI Quanta 200 FEG with a Peltier stage was used for cryo-SEM imaging. An ALP sample in water at pH 10 (ca. 30 μL) was taken as a liquid onto the stage and held for freezing at −20 °C.

Transmission Electron Microscopy (TEM). TEM was performed with an FEI Tecnai G2 F30. Diluted samples were placed on a Lacey mesh ultrathin carbon-coated copper grid. A 2% (w/v) uranyl acetate solution was used to stain organic nanostructures. A diluted sample solution (10 μL) was dropped on a grid for 1 min. The excess amount was removed by pipetting. Then, the 2% uranyl acetate solution was placed on a sheet of parafilm. The grid was placed on the drop upside down for 5 min. After being stained, the grids were dried in the fume hood at room temperature overnight. Inorganic samples were formed on steel meshes by calcination. After calcination, those meshes were put into 1 mL of ethanol and vigorously sonicated for 5 min to disperse inorganic samples in the ethanol. Then 2 μL of the dispersion in ethanol was taken on the TEM grid.

X-ray Diffraction Spectroscopy (XRD). The ALP gel (50 mg) formed in 5 mL of ethanol (1.33×10^{-2} M). Ti(O-*i*-Pr)$_4$ was added as a titania precursor, and the sample was calcined in an alumina crucible at 450 °C. The XRD measurement was performed on the obtained sample by with a Panalytical X-Pert MPD Pro multipurpose X-ray diffractometer. The measurement was performed between 10 and 90° with a step size of 0.0066°.

Thermal Gravimetric Analysis (TGA). A TA Instruments TGA Q500 was used with a heating rate of 20 °C per min. Peptide powder (5 mg) was used for TGA analysis.

Polarized Light Microscopy. An Axio Imager A1m optical microscope was used with two light polarizers. A drop of a 1.33×10^{-2} M peptide sample was sealed between two sliders and characterized with a polarized light microscope.

Oscillatory Rheology. Rheology measurements were performed with an Anton Paar Physica RM301 rheometer operating with a 25 mm parallel plate configuration at 25 °C. Each sample of 100 μL total volume with a final peptide concentration of 1.33×10^{-2} M was carefully loaded onto the center of the lower plate and left untouched for 15 min before measuring. After equilibration, the upper plate was lowered to a gap distance of 0.5 mm. Storage modulus (G') and loss modulus (G'') values were scanned in a time-dependent manner for 75 min with a constant shear strain of 0.5% at a10 rad/s angular frequency.

Critical-Point Dryer. Samples were dried at the critical point (1072 psi, 31 °C) with the Tousimis Autosamdri-815 B series C critical-point dryer.

Results and Discussion

The ALP structure was inspired by amyloid proteins composed of extended sheetlike peptide secondary structures. The ALP molecule was designed to form an extended hydrogen-bonded supramolecular nanostructure. An enhanced stability of the resulting supramolecular nanostructure was achieved by the

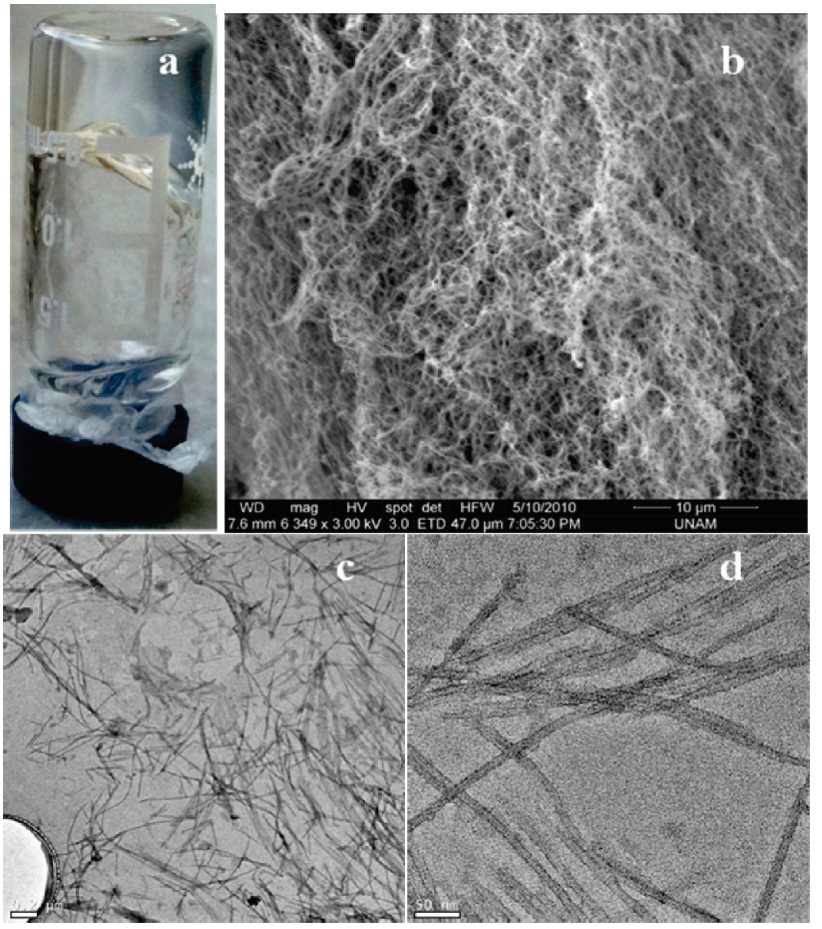

Figure 2. (a) Photograph of the ALP gel (1.33×10^{-2} M in ethanol). (b) SEM image of the ALP gel coated with 3 nm Au/Pd; the scale bar is 10 μm. (c, d) TEM images of peptide nanofibers. Scale bars are (c) 0.2 μm and (d) 50 nm.

incorporation of amino acid residues that provide a directional and relatively strong intermolecular interaction, namely, hydrogen bonding.[22] A diphenylalanine motif was employed to promote β-sheet formation[23] through $\pi-\pi$ stacking.[24] The amine groups on the side chain of lysine residues were used at both ends to functionalize the periphery of the nanostructures. Amines were exploited to seed metal ions around the nanofibers. Also, owing to their basic properties, they are able to catalyze the nucleation of the silica precursor around the organic nanostructures.

The solubility of the ALP molecule was tested in various solvents. A solubility test was performed by adding different amounts of peptide to solvents, and the concentration of 1 mg of peptide in 100 μL of solvent turned out to be the minimum gelation concentration (1.33×10^{-2} M) for water (at pH 10) and ethanol because at this concentration the peptide could completely gel the medium with no residual solvent residing at the top of the gel. The ALP molecule readily dissolved in methanol and in water. The initial pH of the aqueous solution was 5. A 1 M NaOH solution (10 μL) was added to the aqueous solution to raise the pH for the neutralization of charges on amine groups to promote self-assembly. Self-supporting gel formation was observed at pH 10. In addition, the ALP molecule in ethanol also formed a gel after sonication at room temperature (Figure 2a). The solubility of the ALP molecule was also tested in hexane, dichloromethane, acetone, toluene, benzene, tetrahydrofuran, and acetonitrile. The peptide remained as a white precipitate in these solvents even after sonication for 30 min and heating up to 50 °C.

Gel formation was investigated by oscillatory rheology measurements (Figure S3). The storage modulus (G') and the loss modulus (G'') were recorded as a function of time. The values of the storage modulus remained significantly higher than the loss modulus during the measurement, thus supporting a visual evaluation of the mixture as a gel. Self-supporting gel formation was observed for both gels in ethanol (Figure S3a) and in H_2O at pH 10 (Figure S3b). The gel strength increases with time because of changes in G' and G'' with time related to gel aging and solvent evaporation.

The ALP gels in ethanol were composed of a 3-D network of nanostructures as observed by SEM (Figures 2b and S4a−d). According to TEM images, the diameters of the ALP nanofibers were about 15 nm and the length was in the micrometer range (Figures 2c,d and S4e,f). The ALP gel in water at pH 10 also contained nanofibers with diameters similar to the ones in ethanol (Figure S4a,b). The gels were also observed by cryo-SEM, and the gels were composed of a 3-D network of nanofibers, confirming the structures observed by the critical-point-dried gels (Figure S5c−e). The gels were also characterized under a polarized microscope. Figure 3 shows optical micrographs of the gels located between two crossed visible-light polarizers. A characteristic

(22) Parkin, I. P. *Appl. Organomet. Chem.* **2001**, *15*, 236.
(23) Mazor, Y.; Gilead, S.; Benhar, I.; Gazit, E. *J. Mol. Biol.* **2002**, *322*, 1013–1024.
(24) Gazit, E. *FASEB J.* **2002**, *16*, 77–83.
(25) Pomerantz, W. C.; Yuwono, V. M.; Pizzey, C. L.; Hartgerink, J. D.; Abbott, N. L.; Gellman, S. H. *Angew. Chem., Int. Ed.* **2008**, *47*, 1241–1244.
(26) Han, T. H.; Kim, J.; Park, J. S.; Park, C. B.; Ihee, H.; Kim, S. O. *Adv. Mater.* **2007**, *19*, 3924–3927.

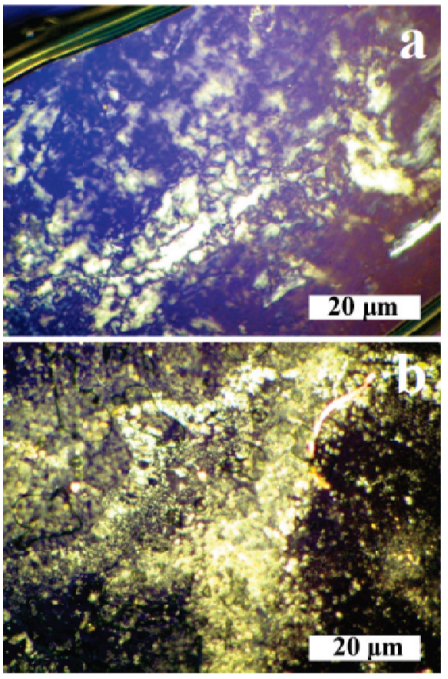

Figure 3. Birefringence effect of self-assembled ALP nanostructures (a) in ethanol and (b) in H_2O at pH 10.

Schlieren texture[25] of the lyotropic liquid-crystal phase was observed in the ALP gels.[26,27]

We investigated UV absorption properties of the ALP in ethanol, methanol, and H_2O at pH 5 and 10. We observed absorption at around 260 nm (Figure S6a,b) in all solvents, which is the characteristic absorption band of phenylalanine residues.[28−30] The self-assembly process triggered by the pH change from 5 to 10 causes a decrease in molar absorptivity; this observation is not surprising because the gelation process results in the formation of nanofibers, which can increase the incident beam scattering. The orientation of phenyl rings is not less important because the fiber-formation process inevitably forces phenylalanine residues to end up inside the fiber body, consequently decreasing the amount of incident radiation being absorbed by the phenylalanine residues.

The fluorescence emission properties of the ALP molecules were also investigated. The fluorescence emission of the peptide in ethanol, methanol, and H_2O at pH 5 and 10 observed upon the excitation of adjacent phenylalanine residues at 260 nm is presented in Figure S7. Two emisson bands can be observed: one with a maximum at 283 nm (monomer)[31] and an additional red-shifted emission band centered at 304 nm. Observed double fluorescence is indicative of excited dimer (excimer) formation due to $\pi-\pi$ interactions.[32−34] The peak at 304 nm was assigned to the excimer. To understand whether excimer formation stems from

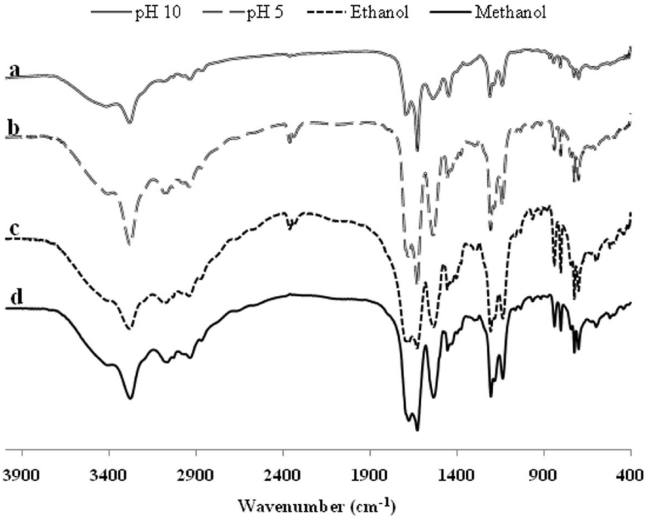

Figure 4. FT-IR spectra of the ALP samples (a) in H_2O at pH 10, (b) in H_2O at pH 5, (c) in ethanol, and (d) in methanol.

intermolecular or intramolecular interactions, some UV−vis and fluorescence measurements were performed with the addition of guanidinium chloride, trifluoroethanol, and hexafluoroisopropanol, respectively (Figures S8, S9, and S10). These molecules were used to completely prevent hydrogen bonding among the peptide molecules, thus excluding the possibility of intermolecular excimer formation. Fluorescence measurements of solutions containing the aforementioned additives have shown that excimer formation is mainly intramolecular. Excimer formation probably takes place because of the proximity of two phenylalanine residues. Some difference between the fluorescence spectra of dissolved peptide at pH 5 and the self-assembled peptide at pH 10 was observed; the former had an attenuated emission peak at 304 nm. The decrease in peak intensity was attributed to the decrease in the extent of excimer formation. Conformational constraints dictated by supramolecular organization probably have an effect on the degree of excimer formation.

FT-IR measurements were performed with dried samples of the ALP solutions in ethanol, methanol, and water at pH 5 and 10 (Figure 4). An amide-A (associated with the −NH stretching frequency) band was observable at around 3296 cm^{-1} in methanol and in H_2O at pH 5, where the ALP was completely dissolved, which is attributed to the −NH group of the peptides involved in hydrogen bonding.[35,36] The amide-A band was at around 3325 cm^{-1} in ethanol and in H_2O at pH 10, where the ALP molecules formed a gel because of self-assembly. Also, amide-I (indicating the existence of C═O stretching vibrations[37,38]) generates two peaks at around 1687 and 1633 cm^{-1}. The splitting of the peak can be due to the interactions between repeating peptide units.[35] The amide-I peak of the ALP in ethanol and in H_2O at pH 10 was found at around 1706−1645 cm^{-1}.

Circular dichroism (CD) measurements were performed to study the effect of peptide secondary structures on nanostructure formation in varying concentrations and solvents (Figures 5a,b and S11). The ALP molecules formed a gel in ethanol and in H_2O at pH 10 and were soluble in H_2O at pH 5 and methanol. The CD signals around 235 and 220 nm indicate β-sheet structure in H_2O

(27) Hamley, I. W. *Soft Matter* **2010**, *6*, 1863–1871.
(28) Murphy, K. P. *Protein Structure, Stability, and Folding*; Humana Press: Totowa, NJ, 2001.
(29) Krysmann, M. J.; Castelletto, V.; Kelarakis, A.; Hamley, I. W.; Hule, R. A.; Pochan, D. J. *Biochemistry* **2008**, *47*, 4597–4605.
(30) Krysmann, M. J.; Castelletto, V.; McKendrick, J. E.; Clifton, L. A.; Hamley, I. W.; Harris, P. J. F.; King, S. M. *Langmuir* **2008**, *24*, 8158–8162.
(31) Teale, F. W.; Weber, G. *Biochem. J.* **1957**, *65*, 476–482.
(32) Albelda, M. T.; García-España, E.; Gil, L.; Lima, J. C.; Lodeiro, C.; Seixas de Melo, J.; Melo, M. J.; Parola, A. J.; Pina, F.; Soriano, C. *J. Phys. Chem. B* **2003**, *107*, 6573–6578.
(33) Yoo, H.; Yang, J.; Yousef, A.; Wasielewski, M. R.; Kim, D. *J. Am. Chem. Soc.* **2010**, *132*, 3939–3944.
(34) Rettig, W.; Paeplow, B.; Herbst, H.; Mullen, K.; Desvergne, J.-P.; Bouas-Laurent, H. *New J. Chem.* **1999**, *23*, 453–460.
(35) Doyle, B. B.; Bendit, E. G.; Blout, E. R. *Biopolymers* **1975**, *14*, 937–957.
(36) Chang, M. C.; Tanaka, J. *Biomaterials* **2002**, *23*, 4811–4818.
(37) Haris, P. I.; Severcan, F. *J. Mol. Catal. B: Enzym.* **1999**, *7*, 207–221.
(38) Barth, A. *Prog. Biophys. Mol. Biol.* **2000**, *74*, 141–173.
(39) Xu, X.-D.; Chen, C.-S.; Lu, B.; Cheng, S.-X.; Zhang, X.-Z.; Zhuo, R.-X. *J. Phys. Chem. B* **2010**, *114*, 2365–2372.

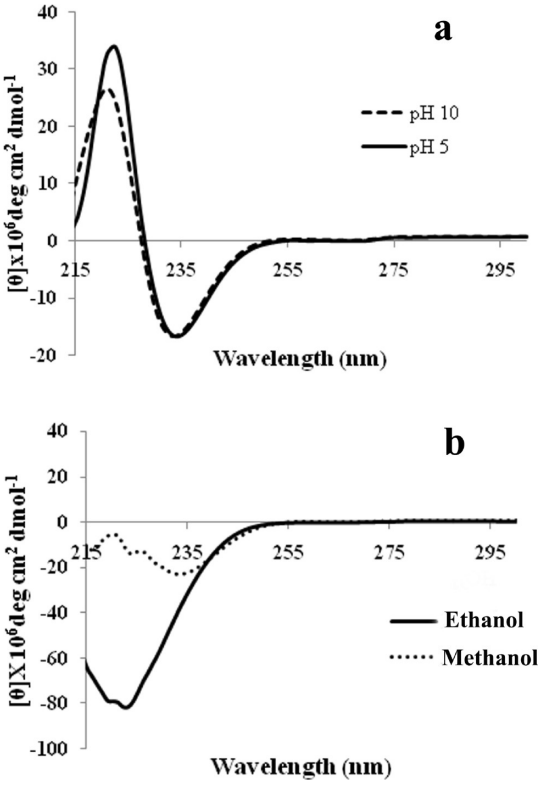

Figure 5. CD spectra of the ALP (a) in H_2O at pH 10 and 5 and (b) in methanol and ethanol.

at both pH 10 and 5 (Figures 5a and S11). The typical β-sheet structure reveals signals at 195 and 216 nm.[39,40] The red-shifted signals indicate that the predominant secondary structure forming the nanostructures is a twisted β-sheet.[41] The CD spectrum of the ALP sample in ethanol reveals a higher intensity than in methanol because of the higher degree of aggregation composed of the twisted β-sheet secondary structure (Figure 5b). The CD (Figure 5) and FT-IR (Figure 4) spectra of the ALP samples are indicative of β-twist and β-turn structures of the self-assembled ALP molecules.

The self-assembled ALP nanostructures were exploited for the template-directed synthesis of titania and silica nanostructures. Titanium[23] isopropoxide [Ti(O-*i*-Pr)$_4$] (5 mol equiv) was used as a titanium precursor along with the self-assembled ALP nanostructures in ethanol. The sample was incubated for 1 h at room temperature, and 100 μL of the sample was cast on a steel mesh and dried with a critical-point dryer. Ti(O-*i*-Pr)$_4$-coated and dried ALP nanostructures were calcined to remove the organic portion and to produce the anatase form of titania. We performed TGA under N_2 and O_2 atmospheres to determine the optimum temperature for the calcination process (Figure S12). The evaporation of the organic content begins above 300 °C. Thus, all of the samples were calcined above 300 °C. Titania samples were calcined at 450 °C to form the anatase phase of titania. After calcination, the formation of the titania hollow nanotubes was observed by TEM (Figures 6 and S17) and SEM (Figure S16). Titanium and oxygen peaks were observed upon SEM/EDX measurement of the calcined samples on a silicon wafer (Figure S13). The silicon peak was high because of the utilization of the silicon wafer. The absence of carbon and nitrogen peaks indicated that the calcination process was mostly completed (Figure S13).

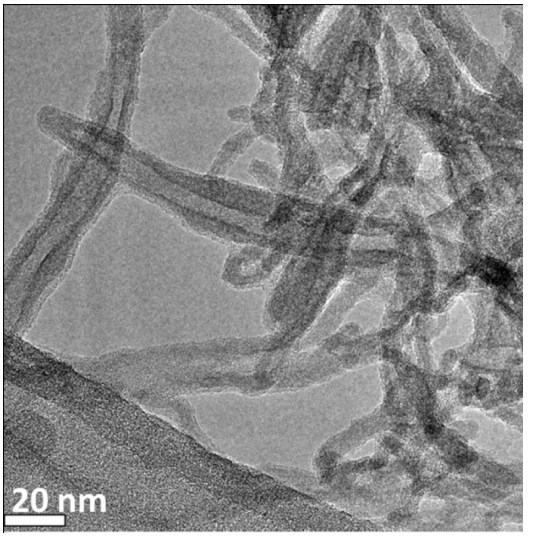

Figure 6. TEM images of the calcined titania nanotubes.

Titania nanotubes were also found to be in the anatase phase[42,43] by XRD measurements (Figure S15). The Ti(O-*i*-Pr)$_4$ precursor was also processed without the ALP to observe the effect of template-directed synthesis, and no defined structures were observed without the template (Figure S20).

Silica mineralization was performed by using tetraethyl orthosilicate (TEOS) as a precursor. TEOS (2 mol equiv) was used along with the ALP nanostructures in ethanol. The TEOS-containing ALP gel was aged for 1 week. Later, the samples were dried with a critical-point dryer and placed in an oven for calcination. The sample was calcined at 350 °C for 10 min. The silica nanostructures after calcination were observed by TEM (Figures 7 and S19) and SEM (Figure S18). The EDX spectra of the calcined silica nanostructures did not reveal carbon and nitrogen signals (Figure S14). In general, silica nucleation from TEOS occurs in the presence of catalysts.[44,45] The amine groups of the ALP molecule acted as a base and started the nucleation of silica on the nanostructures. Therefore, no other catalyst was needed for silica formation. The TEOS precursor was also processed without the ALP to observe the effect of template-directed synthesis, and no defined structures were observed without the template (Figure S21).

During the formation of the inorganic nanostructures, the nucleation process is an important mechanism in shape and size control. We observed that inorganic materials grow on the organic template with the help of the chemically active groups. When the concentration of the template is high enough, the individual organic nanostructures were found to interact and bundle. Therefore, inorganic material grows on the uncontrolled organic aggregate as observed by SEM and TEM (Figures 6, S16, and S18) because of the Ostwald ripening mechanism, which occurs spontaneously because larger particles are more energetically favored than smaller ones.[46−48] During the calcination process, inorganic nanostructures were found to fuse because of

(40) Kubelka, J.; Keiderling, T. A. *J. Am. Chem. Soc.* **2001**, *123*, 12048–12058.
(41) Pashuck, E. T.; Cui, H.; Stupp, S. I. *J. Am. Chem. Soc.* **2010**, *132*, 6041–6046.
(42) Zhang, Y.; Jiang, L. *J. Phys.* (*Paris*) **2009**, *188*, 012004.
(43) Djerdj, I.; Tonejc, A. M. *J. Alloys Compd.* **2006**, *413*, 159–174.
(44) Venkateswara Rao, A.; Bhagat, S. D. *Solid State Sci.* **2004**, *6*, 945–952.
(45) Kang, S.; Hong, S. I.; Choe, C. R.; Park, M.; Rim, S.; Kim, J. *Polymer* **2001**, *42*, 879–887.
(46) Finsy, R. *Langmuir* **2004**, *20*, 2975–2976.
(47) Wilson, G. J.; Matijasevich, A. S.; Mitchell, D. R. G.; Schulz, J. C.; Will, G. D. *Langmuir* **2006**, *22*, 2016–2027.
(48) Ratke, L.; Voorhees, P. W. *Growth and Coarsening: Ostwald Ripening in Materials Processing*; Springer: New York, 2002.

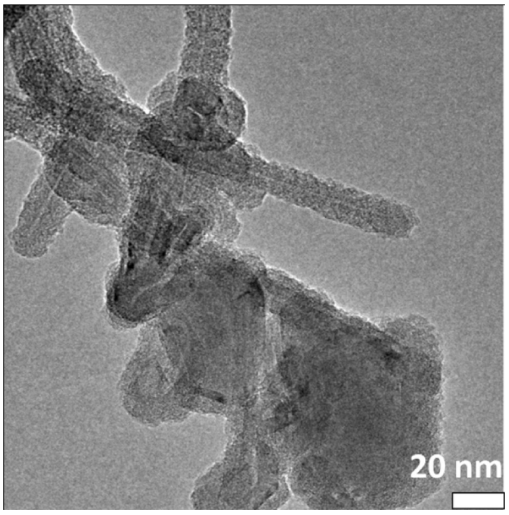

Figure 7. TEM images of the silica nanotubes after calcination.

the high temperature used. The fusion process was observed by SEM (Figures S16 and S18) and TEM (Figures S17 and S19) after the calcination of both silica and titania nanostructures. The uncontrolled growth and fusion of nanostructures could decrease the surface area of the material during calcination.[49,50] To overcome the fusing of the nanostructures, 3-D networks were protected by critical-point drying. The nanostructures were isolated from each other before calcination. By this process, the space between nanofibers was preserved. A higher yield of individual nanostructures was obtained by decreasing the time of calcination and preserving the space between nanofibers.

Conclusions

Herein, we demonstrated a new bottom-up approach to the formation of silica and titania nanostructures by mimicking the biomineralization process with synthetic-peptide-based nanostructures. The self-assembly process was used to form the template, and the mineralization process revealed the controlled formation of inorganic nanostructures. We fabricated silica and titania nanostructures by using a template-directed bottom-up synthesis method. These high-aspect-ratio inorganic nanostructures have vast potential in catalysis and electronic materials. Dye-sensitized solar cells are an interesting field in which the titania nanostructures may enhance the efficiency of the energy conversion by increasing the surface area.[51] Silica nanotubes with high surface areas are especially interesting for use in catalysis.[52,53] Mimicking the natural biomineralization process by means of this kind of simple and controllable self-assembling molecules can be an interesting way to produce bulk amounts of inorganic nanostructures for various industrial and technological applications.

Acknowledgment. This work is supported in part by Marie Curie IRG grant 231019 and TÜBİTAK grant 109T603. We thank Z. Erdogan for help with LC-MS, M. Guler for help with TEM, K. Mizrak for help with SEM/EDX, S. Toksoz for help with rheology, and Prof. M. Toprak and O. O. Ekiz for fruitful discussions.

Supporting Information Available: Additional chemical, spectroscopic, and imaging characterization data. This material is available free of charge via the Internet at http://pubs.acs.org.

(49) Tsantilis, S.; Briesen, H.; Pratsinis, S. E. *Aerosol Sci. Technol.* **2001**, *34*, 237–246.
(50) Xiong, Y.; Kamal Akhtar, M.; Pratsinis, S. E. *J. Aerosol Sci.* **1993**, *24*, 301–313.
(51) Ghadiri, E.; Taghavinia, N.; Zakeeruddin, S. M.; Grätzel, M.; Moser, J.-E. *Nano Lett.* **2010**, *10*, 1632–1638.
(52) Kageyama, K.; Tamazawa, J.-i.; Aida, T. *Science* **1999**, *285*, 2113–2115.
(53) Mitchell, D. T.; Lee, S. B.; Trofin, L.; Li, N.; Nevanen, T. K.; Söderlund, H.; Martin, C. R. *J. Am. Chem. Soc.* **2002**, *124*, 11864–11865.